Compact modeling of a magnetic tunnel junction based on spin orbit torque

Kotb Jabeur, Gregory Di Pendina, Guillaume Prenat, Liliana Daniela Buda-Prejbeanu, Bernard Dieny

Compact Modeling of a Magnetic Tunnel Junction Based on Spin Orbit Torque

Kotb Jabeur, Gregory Di Pendina, Guillaume Prenat, Liliana Daniela Buda-Prejbeanu, and Bernard Dieny, *Fellow, IEEE*

SPINTEC, 38054 Grenoble Cedex 9, France

High endurance, high speed, scalability, low voltage, and CMOS-compatibility are the ideal attributes of memories that any integrated circuit designer dreams about. Adding non-volatility to all these features makes the magnetic tunnel junctions (MTJs) an ultimate candidate to efficiently build a hybrid MTJ/CMOS technology. Two-terminal MTJs based on spin-transfer torque (STT) switching have been intensively investigated in literature with a variety of model proposals. Despite the attractive potential of the STT devices, the issue of the common writing/reading path decreases their reliability dramatically. A three-terminal MTJ based on the spin-orbit torque (SOT) approach represents a pioneering way to triumph over current two-terminal MTJs by separating the reading and the writing paths. In this paper, we introduce the first compact model, which describes the SOT-MTJ device based on recently fabricated samples. The model has been developed in Verilog-A language, implemented on Cadence Virtuoso platform and validated with Spectre simulator. For optimized simulation accuracy, many experimental parameters are included in this model. Simulations prove the capability of the model to be efficiently used to design hybrid MTJ/CMOS circuits. Innovative logic circuits based on the SOT-MTJ device, modeled in this paper, are already in progress.

Index Terms— **Magnetic tunnel junction (MTJ), modeling, MRAM, spin orbit torque (SOT), spintronics, Verilog-A.**

I. Introduction

CURRENT researches in spintronics are investigating a variety of magnetic memory devices, which are promising candidates to improve the capability of existing RAMs by adding one key feature, the non-volatility (NV), and replace them as a long-term purpose, once they reach the maturity stage. For the first generation of the NV MRAMs, the switching mechanism was controlled by applying external magnetic fields. The approach is known as field-induced magnetic switching (FIMS) [1]. It suffers from selectivity and scalability issues. The selectivity issues were partially solved by the so-called toggle approach proposed in [2], but field-based writing schemes remain hardly scalable below 90 nm. Then came the thermally assisted switching (TAS), which allowed solving the selectivity issues while reducing the writing energy and improve the scalability [3].

Both consist of a magnetic tunneling junction (MTJ) as a storage element and require high writing current and consequently increased power consumption and die area due to large transistors and huge write lines. In addition, magnetic-field-based MTJs suffer from the lack of robustness against downscaling. Furthermore, more advanced writing scheme has been proposed to solve the latter issues; spin polarized current can be used through the junction to apply spin transfer torque (STT) [4], [5] and switch the magnetization of the storage layer. Although the writing current has been decreased by orders of magnitude and the scalability issue is solved, two main shortcomings are still limiting the reliability and endurance of STT-MRAMs: 1) in large-scale memories, the high current density required for writing can occasionally damage the MTJ barrier and 2) since writing and reading operations share the same path (through the junction), it remains a challenge to fulfill a reliable reading without ever causing switching.

To solve the latter issues and ensure a continuous advance of MRAM, an interesting phenomena known as spin-obit coupling can be exploited to create a torque on the storage layer magnetization and switch it [6]. The two fundamental physical phenomena responsible for the spin-orbit-torque (SOT) switching mechanism are the Rashba effect [6], [7] and the spin Hall effect (SHE) [8], [9].

In [10], the Rashba spin orbit coupling effect has been utilized to model and design a non-volatile memory with higher spin torque efficiency because of the spin injection free device. In addition, the switching of perpendicularly magnetized ferromagnetic layer based on spin-orbit interactions was reported in [6] and [7]. Then, Liu *et al.* [8] have confirmed the attracting potential of spin-orbit interaction to build magnetic devices favorable for logic storage. Because of its three-terminal architecture, Miron *et al.* and Liu *et al.* [7], [9] claim that SOT switching devices can be built with independent reading and writing paths and so avoid challenges encountered with the state of the art of conventional STT MRAM, whereas keeping competitive switching currents.

As the semiconductor industry is progressively going toward hybrid CMOS integrated circuits, compact model development has become a cornerstone in the circuit/system verification tool flow. By view of this fact and in order to make in evidence the prospective of the SOT magnetic device, it becomes a fundamental step to define a compact model for the SOT device to be used for design purposes based on magnetic storage logic. To the best of our knowledge, this paper represents the first macro-model written in Verilog-A of the

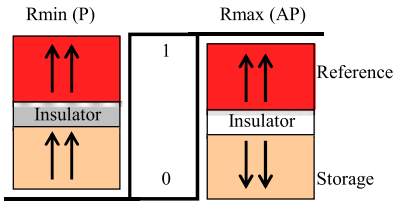

Fig. 1. Resistance variation of the MTJ according to the storage layer magnetization state.

SOT-MTJ. The model describes the behavior of the three-terminal SOT device and includes the dynamic behavior described by the Landau–Lifshitz–Gilbert model (LLG) [11]. To follow the variation of the SOT-MTJ resistance, Julière's model [12] as well as Simmons's model [13] were used in the expression describing the conductance through the junction. Moreover, for an improved accuracy, we integrated the dynamic conductance given by Brinkman model [14] and we took in consideration the dependence of magnetoresistance on bias voltage. Finally, a special interest has been given to Rashba effect and SHE torques inside the LLG equation to highlight the impact of these two factors on the dynamic of magnetization switching intensively argued in [7]–[9].

This paper is organized as follows. In Section II, we present the SOT-MTJ device as well as its switching mechanism. Then, in Section III, a description of the compact model is given. Section IV represents the simulation results and discussions. Finally, we conclude this paper in Section V.

II. Magnetic Tunnel Junction

A. Basics

The MTJs are used as the basic memory elements in MRAM cells and magnetic logic devices. The MTJ is a nanostructure composed of two ferromagnetic layers (FM), such as cobalt, iron, or nickel, separated by a thin layer of insulator typically alumina oxide or magnesium oxide, which represents the tunnel barrier. The first FM layer (hard layer)—with a pinned magnetization—acts as a reference, whereas the second FM layer (soft layer)—with a free magnetization—acts as a storage layer.

The magnetization of the storage layer can be switched between two stable states, either parallel (P) or antiparallel (AP) with respect to the reference layer. Electrons can tunnel through the thin barrier ($\sim$1 nm) when a bias voltage is applied between the two electrodes of the device. The MTJ resistance is low (or high) for a P (or AP) magnetization configuration. These two configurations can be used to code two different logic states, logical 0 and 1, for instance (Fig. 1). This resistance variation behavior was first observed and explained in [12]. Tunnelling magnetoresistance ratio (TMR) describes the ratio between the two resistance values as

$$\mathrm{TMR} = \frac{R_{\mathrm{AP}} - R_P}{R_P}. \tag{1}$$

The highest effects observed to date with aluminum oxide insulators are $\sim$70% at room temperature. The highest TMR recorded in literature is up to 600% at room temperature and $>$1100% at 4.2 K observed in junctions of CoFeB/MgO/CoFeB [15]. A MTJ with a large TMR value offers an accurate read of the output signal. Indeed, for memory applications, we can use a single MTJ memory cell or two MTJs, which have opposite magnetic states, to store one data bit [5]. In both cases, the fact to have a large TMR eases the reading process, which is, most of the time, based a differential approach [16], [17].

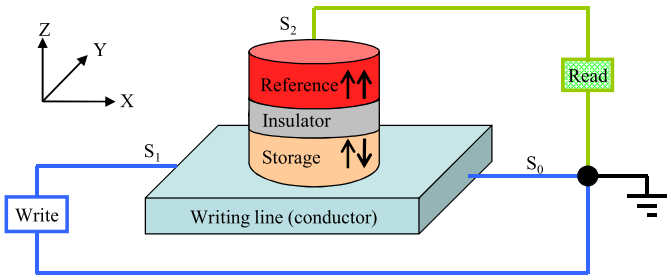

Fig. 2. Schematic view of the three-terminal SOT device and the two independent paths for READ and WRITE operations.

B. SOT-Based MTJ

As mentioned in the introduction, the first generations of the MTJ relying on the Oersted field (generated by an injected current in the writing line) suffer from high writing current, die area, and lack of scalability. Although STT-based MTJ has solved the scalability problem, the common READ/WRITE path through the junction can cause barrier damaging during the writing operation and the switching of the magnetic state during the reading operation. A representative geometry of a three-terminal memory cell with the perpendicular switching of the magnetized FM layer using the SOT writing mechanism is shown in Fig. 2. The structure consists of a three layers nanopillar on the top of a conductor (metal electrode). For clarity reasons, we present only the main layers of the MTJ stack. Additional layers and materials combination could be considered to increase the robustness of the whole structure and mitigate undesirable effects (e.g., dipole fields around the free layer, and so forth). The writing electrode materials existing in literature to fabricate the sample device are β-tantalum (β-Ta) or Pt [7]–[9]. The magnetic cell is written by applying a charge current via the writing line. The orientation of the storage layer magnetization is controlled by the direction of the applied charge current. Positive currents (along x) produce a spin injection current with transverse direction (along z) and spins pointing to y-direction. The injected spin current in-turn produces spin torque to align the magnet in the y or $-y$ direction.

During the time of the applied current pulse, the magnetization of the storage layer is oriented along the y-axis. At the end of the current pulse, the m_z magnetization has an identical probability to be oriented up or down along the z-axis. If there is no external applied field H_a, an arbitrary switching occurs that may be caused by nucleation events [7]. The solution used by research teams working on the realization of the

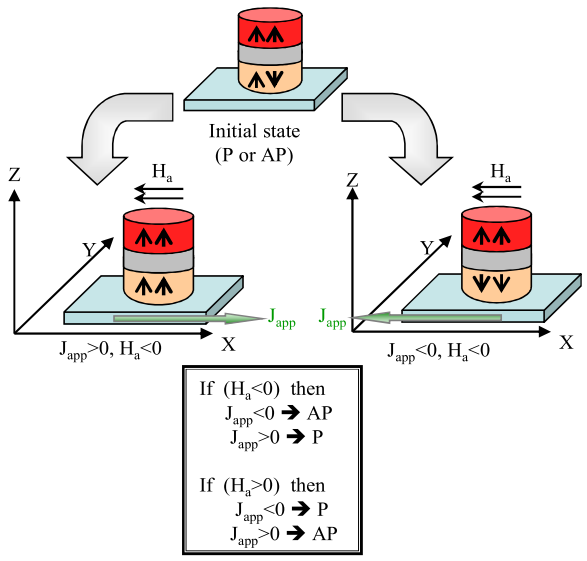

Fig. 3. Switching dependence on the external applied field H_a and the current direction.

SOT device [7]–[9] is the generation of a bias magnetic field H_a by adding a permanent magnet on chip or a biasing layer on top of MTJs. Thus, the magnetic field H_a is permanently present on the top of the MTJ (not only when a current pulse is applied) and it contributes to the control of switching when a pulse of writing current is applied. Fig. 3 illustrates the behavior of the SOT-MTJ in the presence of a permanent magnetic field: starting from the initial magnetization, the AP or P states are obtained by applying a negative current pulse or a positive current pulse, respectively. In Fig. 3, the permanent magnetic field is negative ($H_a < 0$). It is also possible to work with a positive H_a ($H_a > 0$). The effect of the current pulses will be simply inverted, as explained in the pseudocode in Fig. 3. More details about the switching mechanism are available in [7]–[9].

III. Compact Modeling of the SOT Device

A. Modeling Environment and Approximations

Several MTJs compact models have already been published in the literature. While some authors used HSPICE language [18]–[20], others preferred the litheness of C language [21]. There are also several behavioral models Verilog-AMS or VHDL-AMS (both high-level description languages for analog or mixed signal for use with ICCAD tools) that are state-driven, such as the model written in VHDL-AMS [22], [23] or the compact model for (MTJ) switched by thermally assisted STT (TAS + STT) developed in Verilog-A [24].

In this paper, we provide the first compact model written in Verilog-A of a SOT-MTJ. Our choice of the coding language is motivated by the capability of Verilog-A to afford a quick method of enhancing compact models to illustrate new physics of advanced processes. In addition, it is on the path to becoming the preferred compact modeling language for both academic and industrial research groups because of its flexibility to run in numerous simulators (Spectre, HSpice, ADS, Eldo, and so forth) and internal simulators of semiconductor companies. We aim to obtain a straightforward, high-speed, and precise electrical representation of the physical behavior of the SOT-MTJ device. First, we analyze the model equations along with some approximations. Then, because of close interactions with Spintec technologists, a number of associated parameters are fed into these equations. The simulator represents the established equations as equivalent circuit elements. In order to develop this model, we proceed under the macrospin approximation. We consider that the magnetization of each FM layer is uniform (single domain). Hence, it can be described by a single macroscopic magnetic moment. This hypothesis significantly abridges the mathematical analysis. The smaller the sample used, the more pertinent the macrospin assumption is.

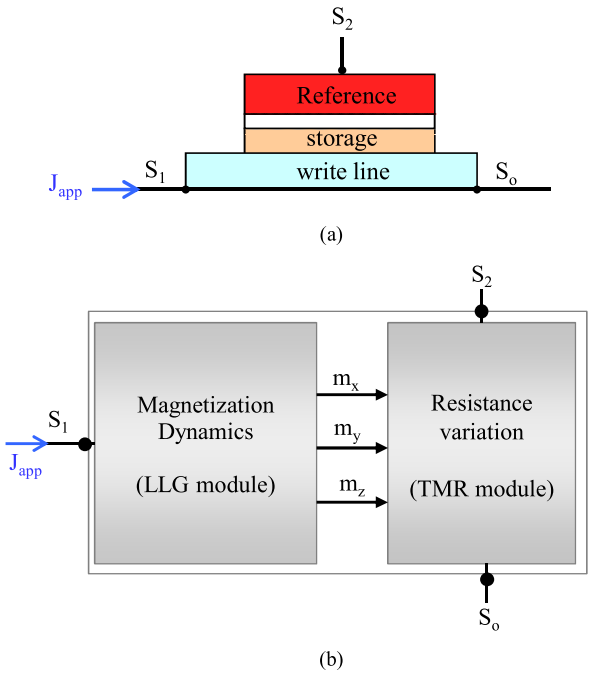

Fig. 4. Modeling strategy of the three-terminal SOT-MTJ. (a) Physical view of the SOT-MTJ (cross section). (b) Block diagram of the compact model.

B. SOT-MTJ Modeling Strategy

The SOT-MTJ model describes the dynamic magnetic behavior of the single domain storage layer as a function of the current density injected through the conductor underneath it.

The physical model of the SOT-MTJ device in Fig. 4(a) illustrates the layers and the signal interface for its input and output signals. Fig. 4(b) gives a block diagram showing all the SOT-MTJ module connections. The whole block diagram is composed of two principal modules: 1) the LLG module and 2) the TMR module.

There are three external nodes (S_0, S_1, and S_2).

1) S_1 and S_0 represent the terminals of the writing path.
2) S_2 and S_0 represent the terminals of the reading path.

The three internal connections are m_x, m_y, and m_z, which correspond to the components of the storage layer magnetization.

1) LLG Module: The LLG module describes the dynamic evolution of the storage layer magnetization as a function of

time and applied current density (J_{app}). This module has one input (J_{app}), which represents the current applied through the WRITE line (S_1S_0) of the device to control the magnetization reversal of the storage layer. The three outputs m_x, m_y, and m_z represent the magnetization components in a Cartesian system.

This module implements the LLG equations [11]

$$\frac{\partial \vec{m}}{\partial t} = -\frac{\gamma_0}{1+\alpha^2}(\vec{m} \times \vec{H}_{\text{eff}}) - \alpha\frac{\gamma_0}{1+\alpha^2}\vec{m} \times (\vec{m} \times \vec{H}_{\text{eff}}) \quad (2)$$

where $\vec{m}$ is the unit vector along the magnetization of the soft layer, α is the Gilbert damping constant, γ_0 is the gyromagnetic ratio, and $\vec{H}_{\text{eff}}$ is the effective field.

The first term in (2) describes the precession of the magnetization around the effective magnetic field. The second term in (2) is the Gilbert damping torque, which forces the magnetization to relax toward the effective field.

The effective field is the sum of the different magnetic fields, which acts on the storage layer magnetization

$$\vec{H}_{\text{eff}} = \vec{H}_k + \vec{H}_d + \vec{H}_R + \vec{H}_{\text{SHE}} + \vec{H}_a \quad (3)$$

where H_k is the magnetocrystalline anisotropy field, H_d is the demagnetizing field, H_R is the Rashba field, H_{SHE} is the SHE field, and H_a is the external applied field.

1) The interaction between the magnetic moment and the crystalline lattice is responsible for a privileged direction, in which the magnetization spontaneously aligns itself in the absence of an external field. The equivalent magnetocrystalline anisotropy field is expressed as

$$\vec{H}_k = (2K_u/\mu_0 M_s)m_z\vec{z} \quad (4)$$

where K_u is the uniaxial anisotropy constant, and M_s is the spontaneous magnetization value.

2) Another source of anisotropy in the shape of magnetic nanostructures via the magnetostatic energy. The magnetization always tends to align with the longest dimension of the ellipsoid in magnetic ellipsoidal nanostructures. This effect is described in the model using the following equation:

$$\vec{H}_d = -M_s\,(n_{xx}\vec{m}_x + n_{yy}\vec{m}_y + n_{zz}\vec{m}_z) \quad (5)$$

where n_x, n_y, and n_z are demagnetizing tensor coefficients.

3) The Rashba effect field and the SHE field are the two original components of the total effective field $\vec{H}_{\text{eff}}$, which differ the SOT-MTJ from other MTJ generations (FIMS, TAS, and STT). Their key role in the magnetic switching of FM dots has given birth to a new concept of three-terminal MRAM that we are describing in this paper. Based on the experiments and the interpretations afforded by SPINTEC technologists [6], [7], the Rashba effect and the SHE fields are expressed according to the following equations, respectively:

$$\vec{H}_R = C_R J_{\text{app}}\vec{y} \quad (6)$$

$$\vec{H}_{\text{SHE}} = -C_{\text{SHE}} J_{\text{app}}\vec{m} \times \vec{y} \quad (7)$$

where C_{R} is the Rashba coefficient, C_{SHE} is the SHE coefficient, and J_{app} is the density of current applied in the conductor. The values of these two factors depend on the nature and the dimensions of the SOT-MTJ layers [9], [25].

4) $\vec{H}_a$ is the external applied field required to coexist with Rashba effect and SHE in order to achieve the magnetic reversal of the storage layer. It is a static magnetic field that can be generated by small permanent magnets fabricating on-chip, close or on top of each active dot. We can also envisage adding a bias layer on the top of the MTJ to maintain a static magnetic field with a component according the x-axis. Neither its value nor its exact orientation is critical for the reversal. Very small applied fields suffice to provoke reversal [7]. In our model, we admit that the external applied field is expressed as

$$\vec{H}_a = H_a\vec{x}. \quad (8)$$

2) TMR Module: The second module of the Verilog-A model is the TMR module, which describes the magnetoresistance variation based on the orientation of the storage and reference layers (P/AP). It takes the output of the LLG module as its inputs and it depends basically on the m_x and m_z component of the magnetization as shown below in equation.

Following the first TMR model in [12] and [26], the tunneling conductance is a function of the angle between the magnetizations of the two FM layers. Furthermore, the bias-dependent conductance of the device at 0 K can be derived in the framework of Simmons's model [13] and Brinkman's model [14]. By combining formulas given by these complementary models, we can assume that the total tunneling conductance is given by

$$g(V, m_x, m_z) = \frac{G_{P_0}(1-2\beta V+3\delta V^2)}{1+\left(\frac{1-(m_x\cos\theta_{mhl}+m_z\sin\theta_{mhl})}{2}\right)\left(\frac{\text{tmr}_0}{1+\frac{V^2}{V_h^2}}\right)} \quad (9)$$

where β and δ are tunnel oxide material-dependent constants, G_{P0} is the conductance in P magnetic configuration at 0 V and 0 K usually calculated from Simmons's model. V represents the bias voltage applied across the device and tmr_0 is the TMR under a low bias voltage. V_h is defined as the voltage at which the TMR amplitude has decreased to half of its low bias value ($\text{tmr}(V_h) = \text{tmr}_0/2$). θ_{mhl} corresponds to the angle with the z-axis of the reference layer magnetic state.

The electrical modeling of the LLG module consists of three $\|$ RC circuits correlated between each other's. When it comes to the TMR module, it is considered as a simple resistor with the conductance equation depending on the output of the LLG module as explained in Fig. 4 and illustrated in (9). This technique of the MTJ electrical modeling has been used and detailed in [21]. It showed accurate results with an attractive simulation time.

IV. Simulation Results

In this section, we present simulation results for the MTJ cell run with Spectre simulator under Cadence Virtuoso platform. We also investigate the impact of the current density,

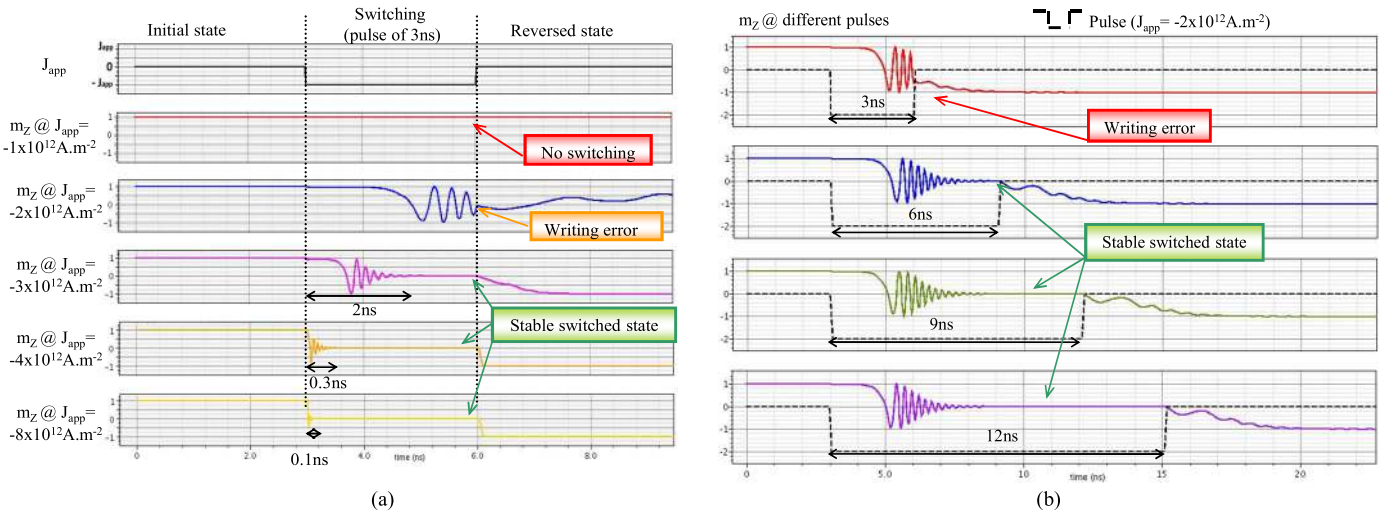

Fig. 5. Study of the dynamic behavior of the perpendicular magnetization m_z according to the variation of the current density J_{app} and the pulsewidth. (a) Evolution of m_z according to the current density J_{app} at 3-ns pulse. (b) Evolution of m_z according to the pulsewidth at $J_{\text{app}} = -2 \times 10^{12}$ A·m^{-2}.

pulsewidth, and external applied field on the behavior of the MTJ dynamics. We note that the following conventions are used in the discussion of simulation results: 1) the initial magnetization state of the SOT-MTJ is in the P state, i.e., the magnetization of the reference layer and the storage layer are along the z-axis with upward orientation (at initial state, we have the perpendicular magnetization along z-axis thus $m_z = 1$); 2) the initial external applied field H_a has a negative value; and 3) negative current pulse switches the MTJ configuration into the AP state, whereas positive pulses switch the MTJ configuration into the P state in the presence of a negative H_a.

A set of experimental-based parameters from [7] and [9] is fed into the model for simulations, among which the geometrical parameters such as the shape, the size, the initial magnetic state of the MTJ, and the other physical and technological parameters. The experiments results delivered by research teams working on SOT devices [6]–[9] claimed that the current density threshold required for switching the magnetization from P (AP) to AP (P) has the same value (symmetrical switching). It is of the order of $J_{\text{app}} = 10^{12}$ A·m^{-2}. We admit that the SHE factor (C_{SHE}) is twice the value of Rashba coefficient (C_R). All this parameters can be easily tuned by the user as current experimental work proceeds.

A. Impact of Current Density and Pulsewidth on the Perpendicular Magnetization m_z

To reverse the perpendicular magnetization (m_z) of the storage layer, a current is applied through the conductor stripe underneath the MTJ structure.

Depending on the width and thickness of the conductor, this current is equivalent to a current density J_{app}, which is the determinant variable in the model to switch the magnetization m_z down (negative J_{app}) or up (positive J_{app}). To find out the required dimensions for the stripe and consequently the writing current, the proper J_{app} must be known in advance. We study in Fig. 5 the dynamic evolution of the m_z component for different values of applied current density (J_{app}) based on the experimental results published for this type of device, which claim that J_{app} must be in the order of 10^{12} A·m^{-2}.

We choose to begin our study with a negative pulse of 3 ns and vary the current density value to observe the dynamics of switching. Fig. 5(a) shows that at $J_{\text{app}} = -1 \times 10^{12}$ A.m^{-2}, the spin torque is not enough to act on the magnetization of the storage layer, the initial state ($m_z = 1$) is retained during and after the pulse. Starting from a value of $J_{\text{app}} = -2 \times 10^{12}$ A.m^{-2}, we can notice the manifestation of a spin torque action on the magnetization. However, because of the shortness of the applied pulse, it was not possible to attain the reversal of the magnetization. The pulse of current ends during precessions (before the stabilization of the m_z) and so we obtain and erroneous writing. If we apply a longer pulse, the magnetization occurs. This is confirmed in Fig. 5(b), where we vary the pulsewidth with a fixed current density of $J_{\text{app}} = -2 \times 10^{12}$ A.m^{-2}. So, when we apply large pulses, a lower current is required for switching. From Fig. 5(a), we notice that the higher is the value of J_{app}, the smaller is the width of the pulse required for switching. For example, at $J_{\text{app}} = -4 \times 10^{12}$ A.m^{-2}, the width of the pulse could be only 0.3 ns instead of the 3 ns applied and could decrease further ($\sim$0.1 ns for $J_{\text{app}} = 8 \times 10^{12}$ A.m^{-2}). To sum up, based on the simulations results, at least a current density of -2×10^{12} A.m^{-2} is required to make the magnetization reversal occur at large pulses ($\sim$6 ns). For higher current density, the required pulsewidth decreases further to attain hundreds of picoseconds starting from a current density of -4×10^{12} A.m^{-2}. These simulation results show a good agreement with experimental measurement [7], where the magnetization switching is achieved at $J_{\text{app}} \sim -2 \times 10^{12}$ A.m^{-2} with a pulsewidth of 9 ns.

B. Impact of the External Field H_a on the Magnetization Reversal

The effective field resulting from the in-plane current injection is orthogonal to the easy magnetization axis (z) and so it cannot control the magnetization reversal by itself. In fact,

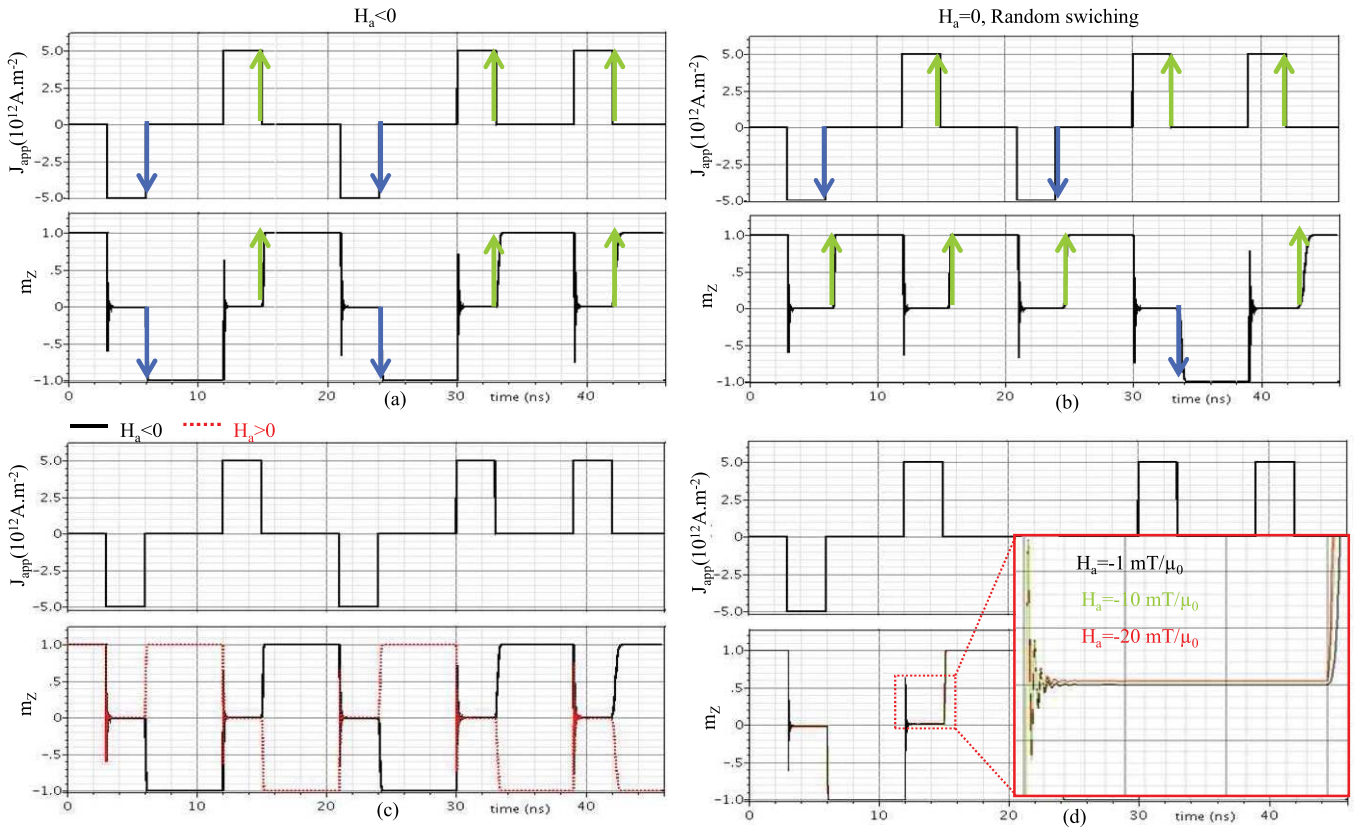

Fig. 6. Study of the dynamic behavior of the perpendicular magnetization m_z according to the variation of the sign and value of the external applied field H_a. (a) Negative value of H_a. (b) Absence of H_a. (c) Opposite behaviour of m_z depending on the sign of H_a. (d) Effect of increasing H_a magnitude.

during the time when the pulse is applied, the magnetization vector m_z oscillates at first till stabilizing at the zero value. Once the pulse is completed, m_z has an identical probability to be oriented up or down along the z-axis. If there is no external applied field H_a, an arbitrary switching occurs that may be caused by nucleation events. Fig. 6(b) illustrates the random switching in the absence of an external magnetic field. In our case, the reversal in one direction or another when $H_a = 0$, is probably due to numerical noise. The solution used by research teams working on the realization of the SOT device [7]–[9], is the generation of a permanent magnetic field H_a by adding a permanent magnet on chip or a biasing layer on top of the MTJs. The field H_a contributes to the control of switching when a pulse of writing current is applied as it is explained in Section II-B in Fig. 3.

Fig. 6(a) shows a proper reversal of the magnetization m_z according to the current pulse in the presence of a negative field. If a negative pulse is applied, the magnetization is reversed downward ($m_z = -1$), whereas a positive pulse switches the magnetization upward ($m_z = 1$). Fig. 6(c) shows that the response to the current direction can also be inverted by reversing the direction of H_a (reversing the polarization of the magnets responsible for the generation of the static magnetic field H_a). Finally, we verified the fact that we do not require high values of applied field to reverse the magnetization as shown in Fig. 6(d), where we used three different values of H_a and observed that the value of applied field is not crucial in the reversal mechanism, a small value is sufficient.

C. Magnetoresistance Variation as a Function of the Applied Current

In Fig. 7, we investigate the variation of the SOT-MTJ as a function of the current pulses applied through the writing line underneath. We fixed the bias voltage at 1 V and we observed the evolution of the current for different pulses.

For the P state ($m_z = 1$), we notice a higher current value of 8.75 μA (i.e., lower resistance) and for the state AP ($m_z = -1$), we notice a lower current value of 7.3 μA (i.e., higher resistance). Thus, the model describes correctly the dependence of the MTJ resistance on the state of the perpendicular magnetization m_z, which in turn depends on pulses of the writing current.

D. Limitations, Advantages and Future of SOT Devices

Based on the simulation results obtained from the compact model, which is in accord with the first experimental characterizations of SOT-MTJs available in literature, we highlight the main drawbacks, the benefits, and the possible improvements concerning the SOT MRAMs. It is worth to point out that the first fabricated devices show a high current density required for the magnetization switching (J_{app} ~2−3 × 10^{12} A.m^{-2}) and consequently a high writing current (>2 mA).

However, researchers working on the SOT concept are optimistic about the future of this device and claim that the current can be decreased with further interface engineering. In [7], the author noted that the in-plane current can be applied

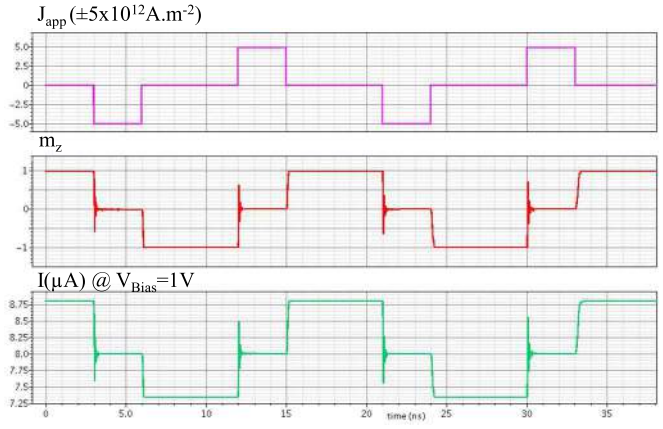

Fig. 7. Validation of the magnetoresistance variation according to writing current pulses.

through a thinner lateral surface, thus the absolute current required for switching can be made very small (∼1 mA). An attractive alternative has been already achieved by Cornell University in [9], where they fabricated a SOT device with the tantalum (Ta) as a microstrip conductor for the writing line instead of platinum. They reported a giant SHE in β-tantalum that generates spin currents intense enough to induce efficient spin-torque switching of ferromagnet at room temperature. Using tantalum, experimental results show that a current of ∼1 mA is required for switching (half the current required with platinum). We predict that it is possible to further decrease the switching current by a factor of 3, if they shrink the width of the Ta microstrip to be equal to the dimension of the long axis of the nanopillar. In addition, they suppose that a further reduction in current could be achieved by reducing the demagnetization field of the FM free layer [28], [29].

Based on all these improvements, the required current for SOT devices could be reduced to <100 μA. At such a current value, three-terminal SOT devices would be very competitive with the efficiency of conventional STT-MTJs [30], [31]. Three-terminal SOT approach can even overstep the two-terminal STT devices since it separates the reading and the writing paths. This enhances the reliability of devices and overcomes the main challenges encountering MRAMs. Although it is still in its infancy, the three-terminal architecture of SOT devices promises efficiency and easiness for the fabrication process. Finally, a giant step toward the perfection of this innovative device could be the discovery of materials with larger values of the spin Hall angle.

V. Conclusion

In this paper, we present the first compact model for a three-terminal MTJ nanopillar switching using the SOT approach, which is expected to enhance reliability and overcome challenges facing the conventional two-terminal STT devices. Transient simulations of the model validate its functionalities and show a good agreement with the fabricated device in literature. This model is written in Verilog-A language, compatible with the Spectre simulator of the standard Cadence design suite and with the majority of known simulators. Furthermore, improvements of the model require additional feedback from technologists working on the SOT-MTJs physics. However, already in its present form, it constitutes a very important tool for the design of complex hybrid CMOS/magnetic architectures and it enables one designer to explore the prospective of SOT devices. Using this model, a number of hybrid MTJ/CMOS logic circuits are under examination in our laboratory with inventive architectures because of the three-terminal structure of the SOT-MTJ.

Acknowledgment

The authors would like to thank G. Gaudin for fruitful discussions. This work was supported by the framework of the Spot Project under Grant n°318144 through the European Commission under the Seventh Framework Programme.

References

[1] S. Wolf *et al.*, "Spintronics: A spin-based electronics vision for the future: Magnetism and materials," *Science*, pp. 1488–1495, 2001.

[2] B. N. Engel, J. Akerman, B. Butcher, R. W. Dave, M. DeHerrera, M. Durlam, *et al.*, "A 4-Mb toggle MRAM based on a novel bit and switching method," *IEEE Trans. Magn.*, vol. 41, no. 1, pp. 132–136, Jan. 2005.

[3] L. Prejbeanu, M. Kerekes, R. C. Sousa, H. Sibuet, O. Redon, B. Dieny, *et al.*, "Thermally assisted MRAM," *J. Phys., Condensed Matter*, vol. 19, no. 16, p. 165218, 2007

[4] E. Deng, Y. Zhang, J.-O. Klein, D. Ravelsona, C. Chappert, and W. Zhao, "Low power magnetic full-adder based on spin transfer torque MRAM," *IEEE Trans. Magn.*, vol. 49, no. 9, pp. 4982–4987, Sep. 2013.

[5] H. Zhao, K. C. Chun, J. D. Harms, T.-H. Kim, J.-P. Wang, and C. H. Kim, "A scaling roadmap and performance evaluation of in-plane and perpendicular MTJ based STT-MRAMs for high-density cache memory," *IEEE J. Solid-State Circuits*, vol. 48, no. 2, pp. 598–610, Feb. 2013.

[6] P. Gambardella and I. M. Miron, "Current-induced spin–orbit torques," *Phil. Trans. R. Soc. A*, vol. 369, no. 1948, pp. 3175–3197, 2011.

[7] I. M. Miron, K. Garello, G. Gaudin, P. J. Zermatten, M. V. Costache, S. Auffret, *et al.*, "Perpendicular switching of a single ferromagnetic layer induced by in-plane current injection," *Nature*, vol. 476, no. 7359, pp. 189–193, Aug. 2011.

[8] L. Liu, O. J. Lee, T. J. Gudmundsen, D. C. Ralph, and R. A. Buhrman, "Current-induced switching of perpendicularly magnetized magnetic layers using spin torque from the spin Hall effect," *Phys. Rev. Lett.*, vol. 109, p. 096602, 2012.

[9] L. Liu, C.-F. Pai, Y. Li, H. W. Tseng, D. C. Ralph, and R. A. Buhrman, "Spin-torque switching with the giant spin hall effect of tantalum," *Science*, vol. 336, no. 6081, pp. 555–558, 2012.

[10] J. Guo, S. G. Tan, M. B. A. Jalil, K. Eason, S. Y. H. Lua, S. Rachid, *et al.*, "MRAM device incorporating single-layer switching via Rashba-induced spin torque," *IEEE Trans. Magn.*, vol. 47, no. 10, pp. 3868–3871, Oct. 2011.

[11] L. Landau and E. Lifshitz, "Theory of the dispertion of magnetic permeability in ferromagnetic bodies," *Phys. Z. Sowjetunion*, vol. 8, no. 153, pp. 153–169, 1935.

[12] M. Julliere, "Tunneling between ferromagnetic films," *Phys. Lett. A*, vol. 54, no. 3, pp. 225–226, 1975.

[13] J. G. Simmons, "Generalized formula for the electric tunnel effect between similar electrodes separated by a thin insulating film," *J. Appl. Phys.*, vol. 34, pp. 1793–1803, Jun. 1963.

[14] W. F. Brinkman, R. C. Dynes, and J. M. Rowell, "Tunneling conductance of asymmetrical barriers," *J. Appl. Phys.*, vol. 41, pp. 1915–1921, Apr. 1970.

[15] S. Ikeda, J. Hayakawa, Y. Ashizawa, Y. M. Lee, K. Miura, H. Hasegawa, *et al.*, "Tunnel magnetoresistance of 604% at 300 K by suppression of Ta diffusion in CoFeB/MgO/CoFeB pseudo-spin-valves annealed at high temperature," *Appl. Phys. Lett.*, vol. 93, no. 8, p. 082508, 2008.

[16] W. Zhao, E. Belhaire, and C. Chappert, "Spin-MTJ based non-volatile flip-flop," in *Proc. IEEE 7th Int. Conf. Nanotechnol.*, Hong Kong, China, Aug. 2007, pp. 399–402.

[17] D. Chabi et al, "Robust neural logic block (NLB) based on memristor crossbar array," in *Proc. IEEE/ACM Int. Symp. Nanosc. Archit.*, San Diego, CA, USA, Jun. 2011, pp. 137–143.

[18] B. Das and W. C. Black, "A generalized HSPICE^{TM} macro-model for pinned spin-dependent tunneling devices," *IEEE Trans. Magn.*, vol. 35, no. 5, pp. 2889–2891, Sep. 1999.

[19] B. Das, W. C. Black, and A. V. Pohm, "Universal HSPICE macromodel for giant magnetoresistance memory bits," *IEEE Trans. Magn.*, vol. 36, no. 4, pp. 2062–2072, Jul. 2000.

[20] S. Lee, S. Lee, H. Shin, and D. Kim, "Advanced HSPICE macromodel for magnetic tunnel junction," *Jpn. J. Appl. Phys.*, vol. 44, pp. 2696–2700, Apr. 2005.

[21] G. Prenat, M. E. Baraji, W. Guo, R. Sousa, L. Buda-Prejbeanu, B. Dieny, *et al.*, "CMOS/magnetic hybrid architectures," in *Proc. 14th IEEE ICECS*, Dec. 2007, pp. 190–193.

[22] T. Sugimura, J. Deguchi, H. Choi, T. Sakaguchi, H. Oh, T. Fukushima, *et al.*, "Low-power and high-sensitivity magnetoresistive random access memory sensing scheme with body-biased preamplifier," *Jpn. J. Appl. Phys.*, vol. 45, no. 4B, pp. 3321–3325, 2006.

[23] M. Madec, J.-B. Kammerer, and L. Hébrard, "Compact modeling of a magnetic tunnel junction—Part II: Tunneling current model," *IEEE Trans. Electron Devices*, vol. 57, no. 6, pp. 1416–1424, Jun. 2010.

[24] W. Zhao, J. Duval, J.-O. Klein, and C. Chappert, "A compact model for magnetic tunnel junction (MTJ) switched by thermally assisted Spin transfer torque (TAS + STT)," *Nanosc. Res. Lett.*, vol. 6, no. 1, p. 368, 2011.

[25] P. M. Haney, H.-W. Lee, K.-J. Lee, A. Manchon, and M. D. Stiles, "Current induced torques and interfacial spin-orbit coupling: Semiclassical modeling," *Phys. Rev. B*, vol. 87, no. 17, pp. 174411-1–174411-13, 2013.

[26] J. C. Slonczewski, "Currents, torques, and polarization factors in magnetic tunnel junctions," *Phys. Rev. B*, vol. 71, no. 2, pp. 024411-1–024411-10, 2005.

[27] W. Guo, G. Prenat, V. Javerliac, M. E. Baraji, N. de Mestier, C. Baraduc, *et al.*, "SPICE modelling of magnetic tunnel junctions written by spin-transfer torque," *J. Phys. D, Appl. Phys.*, vol. 43, no. 21, p. 215001, 2010.

[28] L. Q. Liu, T. Moriyama, D. C. Ralph, and R. A. Buhrman, "Reduction of the spin-torque critical current by partially canceling the free layer demagnetization field," *Appl. Phys. Lett.*, vol. 94, no. 12, pp. 122508-1–122508-3, 2009.

[29] T. Moriyama, T. J. Gudmundsen, P. Y. Huang, L. Q. Liu, D. A. Muller, D. C. Ralph, *et al.*, "Tunnel magnetoresistance and spin torque switching in MgO-based magnetic tunnel junctions with a Co/Ni multilayer electrode," *Appl. Phys. Lett.*, vol. 97, no. 7, p. 072513, 2010.

[30] S. Ikeda, K. Miura, H. Yamamoto, K. Mizunuma, H. D. Gan, M. Endo, *et al.*, "A perpendicular-anisotropy CoFeB–MgO magnetic tunnel junction," *Nature Mater.*, vol. 9, pp. 721–724, Jul. 2010.

[31] T. Kishi, H. Yoda, T. Kai, T. Nagase, E. Kitagawa, M. Yoshikawa, *et al.*, "Lower-current and fast switching of a perpendicular TMR for high speed and high density spin-transfer-torque MRAM," in *Proc. IEEE IEDM*, San Francisco, CA, USA, Dec. 2008, pp. 1–4.